Young's Equation at the Nanoscale

David Seveno,* Terence D. Blake, and Joël De Coninck
Laboratory of Surface and Interfacial Physics, Université de Mons, Place du Parc, 20, 7000 Mons, Belgium
(Received 29 May 2013; published 27 August 2013)

In 1805, Thomas Young was the first to propose an equation to predict the value of the equilibrium contact angle of a liquid on a solid. Today, the force exerted by a liquid on a solid, such as a flat plate or fiber, is routinely used to assess this angle. Moreover, it has recently become possible to study wetting at the nanoscale using an atomic force microscope. Here, we report the use of molecular-dynamics simulations to investigate the force distribution along a 15 nm fiber dipped into a liquid meniscus. We find very good agreement between the measured force and that predicted by Young's equation.

DOI: 10.1103/PhysRevLett.111.096101 PACS numbers: 68.08.Bc, 61.20.Ja, 68.49.Df

As is well known, for a partially wetting liquid in contact with a solid and its vapor at a three-phase contact line, Young's equation [1] predicts that

$$\gamma_{SV} - \gamma_{SL} = \gamma_{LV}\cos\theta^0. \tag{1}$$

Here, γ_{SV}, γ_{SL}, and γ_{LV} are, respectively, the solid-vapor, solid-liquid, and liquid-vapor interfacial tensions and θ^0 is the equilibrium contact angle measured through the liquid. Although thermodynamically sound [2,3], this equation cannot be verified experimentally, since the surface tensions of solids can only be inferred and not measured directly. Partly as a result, but also because of the apparent neglect of the normal component of the surface tension force $\gamma_{LV}\sin\theta^0$, the equation has been periodically challenged [4], and its validity at the nanoscale remains an open question [5,6], although evidence for this was recently demonstrated in a Monte Carlo study of a symmetric binary fluid mixture in a nanoscopic slit pore [7]. Nevertheless, Young's equation now plays a crucial role in nanotechnology, as the contact angle is being used to characterize the interactions of liquids with solids of near molecular dimensions, such as carbon nanotubes [8] and nanocones [9]. However, in these experiments, the equation is used on trust, with limited detailed evidence of its validity for these small systems.

At the nanoscale, a typical contact angle measurement consists of dipping a solid into a liquid and recording the force F acting on the solid using an atomic force microscope (AFM). From a macroscopic thermodynamic perspective, withdrawal of the solid is associated with an increase in the solid-vapor interface and a corresponding decrease in the solid-liquid interface. As a result, the total net force exerted on the solid per unit length of the contact line is

$$\frac{F}{P} = \gamma_{SV} - \gamma_{SL}, \tag{2}$$

where P is the effective perimeter of contact. From Young's equation, it follows that

$$\frac{F}{P} = \gamma_{LV}\cos\theta^0. \tag{3}$$

In order to be sure that this macroscopic thermodynamic model is still justified in AFM measurements, we need to show that the forces are the same in both cases when applied at this scale. However, the situation is not quite as straightforward as Eq. (1) might suggest.

Recent thermodynamic arguments based on our modern understanding of the molecular origin of interfacial tension [10] show that the tangential force exerted by the liquid on a partially immersed smooth solid such as a plate or cylindrical rod is zero everywhere, except at not one but two locations: the three-phase contact line and the base of the solid. This is illustrated in Fig. 1. Furthermore, it turns out that at the contact line, the tangential force exerted by the liquid on the solid is not $\gamma_{SV} - \gamma_{SL}$, as might be expected from Eqs. (1) and (2), but

$$\gamma_{SV} - \gamma_{SL} + \gamma_{LV}. \tag{4}$$

This quantity is equivalent to the reversible work of adhesion between a liquid and a solid Wa^0, which is defined as the energy required to destroy unit area of a solid-liquid interface and create equivalent areas of solid-vapor and liquid-vapor interfaces at constant temperature and pressure. Substituting for $\gamma_{SV} - \gamma_{SL}$ using Eq. (1) gives the Dupré equation [11]

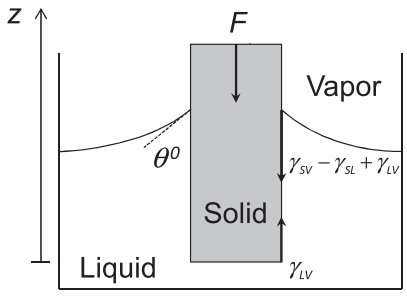

FIG. 1. Schematic illustration of the tangential forces exerted on a partially immersed rod.

 © 2013 American Physical Society

$$Wa^0 = \gamma_{LV}(1 + \cos\theta^0). \quad (5)$$

The existence of the force $\gamma_{LV}(1 + \cos\theta^0)$ at the contact line has recently been confirmed by density functional theory [12] and molecular dynamics [13].

The apparent paradox raised by Eq. (4) is resolved once it is recognized [10,14] that there is an additional force at the base of the solid acting upwards. This is identical to γ_{LV} and arises because of the Laplace pressure generated over the submerged base of the solid. Once this is subtracted from the force at the contact line, Eq. (2) is recovered. Another way of rationalizing this force from the macroscopic thermodynamic standpoint is to notice that as the solid is withdrawn from the liquid and the solid-liquid interface is destroyed, a new liquid-liquid interface is created by bringing together two liquid surfaces, liberating the work of cohesion $2\gamma_{LV}$.

The aim of the work described in this Letter is to investigate the magnitude and distribution of these forces at a scale similar to that of the AFM experiments. To do this, we use large-scale molecular dynamics to simulate the capillary rise of a liquid meniscus around a cylindrical rigid nanofiber, as illustrated in Fig. 2. The simulations allow us to measure the tangential force per unit length exerted by the liquid along the total immersed height of the fiber, together with the equilibrium contact angle. We also measure γ_{LV} in an independent simulation using a planar liquid film. This gives us all the information required to calculate both $\gamma_{SV} - \gamma_{SL}$ and $\gamma_{LV}\cos\theta^0$ in Eqs. (2) and (3) and compare the values obtained.

As we will show, our results do indeed confirm that Eqs. (2) and (3) yield the same result and, therefore, that Young's equation may be applied at this scale. As far as we are aware, the forces exerted by a liquid on a cylindrical nanofiber have not previously been studied by molecular dynamics. In particular, we believe that this is the first time that the force acting at the base of an immersed solid has been resolved and shown to be equal to the surface tension of the liquid and independent of the strength of solid-liquid interactions and the contact angle.

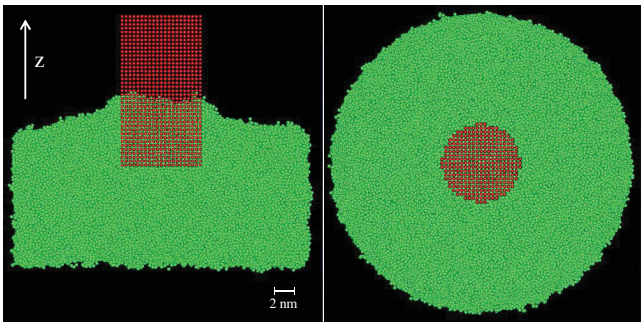

FIG. 2 (color). Front and top views showing our molecular-dynamics simulations of a cylindrical rod (red atoms) dipping into a cylindrical liquid bath (green molecules) held in place within a frozen liquid annulus. The configuration shows the equilibrium configuration for $C_{S-L} = 1.0$.

Simulation model.—The main elements of the simulations, including geometry, potentials, specific parameters, and procedures, are set out below. Most of them have already been applied successfully to study both the statics and the dynamics of wetting for simple liquids in various geometries [15–18]. The key parameters are the potentials between the solid (S) and liquid (L) atoms, which are modeled by standard pairwise Lennard-Jones 12-6 interactions:

$$U(r_{ij}) = 4C_{A-B}\epsilon_{ij}\left[\left(\frac{\sigma_{ij}}{r_{ij}}\right)^{12} - \left(\frac{\sigma_{ij}}{r_{ij}}\right)^{6}\right], \quad (6)$$

where r_{ij} is the distance between any pair of atoms i and j. The coupling parameter C_{A-B} enables us to control the relative affinities between the atoms. The subscript $A - B$ stands for the various possible interaction pairs: L-L, L-S, and S-S. The parameters ϵ_{ij} and σ_{ij} are related, respectively, to the depth of the potential well and an effective atomic diameter. For both solid and liquid atoms, $\epsilon_{ij} = 0.267 \times 10^3$ J/mol and $\sigma_{ij} = 0.35$ nm. The pair potential is set to zero for $r_{ij} = 2.5\sigma_{ij}$. C_{A-B} is given the value 1.0 for L-L and S-S interactions, but the S-L coupling is varied from 0.4 to 1.05 to explore a wide range of equilibrium contact angles. To limit evaporation, the liquid is modeled at a molecular level as eight-atom chains, with a confining potential between nearest neighbors i and j: $U_{\text{conf}}(r_{ij}) = Ar_{ij}^6$. The constant A is set to $\epsilon_{ij}/\sigma_{ij}^6$.

The nanofiber is built as a vertical stack of 39 square lattices and comprises 12 675 atoms, with the distance between atoms initially set to the equilibrium distance given by the Lennard-Jones potential, i.e., $2^{1/6}\sigma_{ij}$. To create a realistic solid, the atoms are allowed to vibrate around their equilibrium positions according to a harmonic potential $U_h(\vec{r}_i) = D \mid \vec{r}_i - \vec{r}_i^{\,0} \mid^2$ with $\vec{r}_i$ the instantaneous position of a solid atom i and $\vec{r}_i^{\,0}$ its initial position. The constant D is set to $2500(\epsilon_{ij}/\sigma_{ij}^2)$. It guarantees that the solid is rigid. The resulting fiber has a height of 15 nm and an effective radial perimeter of 31.4 nm. The masses of both liquid and solid atoms are set to that of carbon (12 g/mol). The time step of the simulation is 5 fs. The successive configurations of the system, i.e., the positions of the atoms, are recorded every 1000 time steps, at a reduced temperature $T^* = k_BT/\epsilon_{ij} = 1.0$. During the simulations, only the temperature of the solid is kept constant, allowing us to mimic an isothermal solid. Our previous work has shown that although this model is simple, it captures the essential physics of wetting.

The liquid bath is a cylindrical annulus with a radius and height of 15 nm; it contains 20 721 eight-atom chains. It is anchored around its circumference by a monolayer of frozen liquid, within which it equilibrates. The nanofiber is positioned just above the meniscus and then partially immersed at a steady velocity, before stopping. The meniscus is allowed

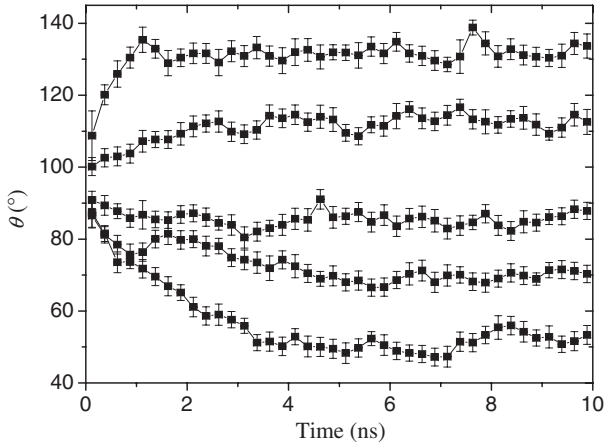

FIG. 3. Contact angle versus time for five different liquid-solid interactions (from top to bottom, $C_{S-L} = 0.4$, 0.6, 0.8, 0.9, and 1.0 with, respectively, $\theta^0 = 133.0° \pm 3.3°$, $108.8° \pm 3.3°$, $85.7° \pm 3.4°$, $70.0° \pm 3.5°$, and $51.0° \pm 3.5°$). Each point is the average of 50 successive values, and the error bars are the standard deviations.

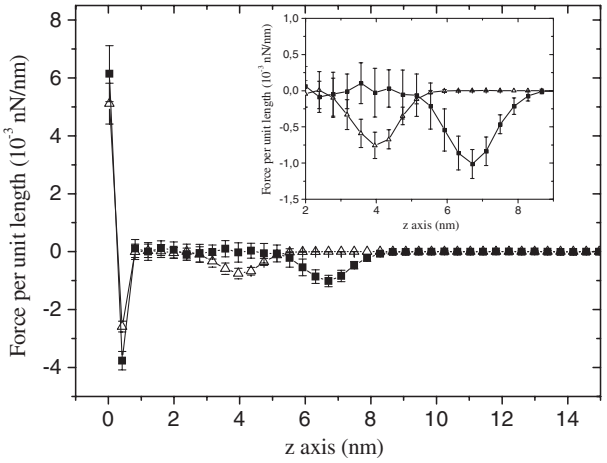

FIG. 4. Tangential force distribution at equilibrium along the nanofiber obtained from the simulations at two solid-liquid couplings: $C_{S-L} = 0.8$ (triangles) and 1.0 (squares). The inset shows an enlarged view of the force distribution at the contact line. The error bars are the standard deviations on the average values of the forces calculated for each layer of the fiber.

to relax until it reaches equilibrium. The static contact angle and the tangential forces exerted by the liquid on the nanofiber in the z direction are then calculated.

Contact angle measurements.—To ensure that equilibrium is reached, we determine the evolution of the contact angle and contact-line position with time as the meniscus relaxes. For each configuration, we locate the liquid-vapor interface by a density calculation and record its position. We then approximate the meniscus shape by a catenoid [17] and fit it to the James equation [19]. Examples of contact angle dynamics observed during meniscus relaxation are illustrated in Fig. 3 for $C_{S-L} = 0.4$, 0.6, 0.8, 0.9, and 1.0. The equilibrium contact angle is obtained once there is no further change with time within the precision allowed by thermal fluctuations.

Interfacial tension measurement.—To determine γ_{LV}, we run independent simulations with a planar liquid film. The interfacial tension is calculated from the pressure tensor using the formula [20,21]

$$\gamma = \frac{1}{2S}\left\langle \sum_{i=1}^{N}\sum_{j>i}^{N}\left(1 - \frac{3r_{ijz}^2}{r_{ij}^2}\right) r_{ij}\frac{\partial U(r_{ij})}{\partial r_{ij}}\right\rangle, \qquad (7)$$

where r_{ijz} is the z component of the separation vector $\vec{r}_i - \vec{r}_j$ and S the area of the film. The sum over all N liquid atoms is such that only the atoms at the interfacial region contribute. The value obtained for γ_{LV} was 2.49 ± 0.5 mN/m.

Force measurements.—The forces exerted by the liquid on the nanofiber are obtained by differentiation of Eq. (6) for the Lennard-Jones potential between the fiber and liquid atoms. The calculations are done once the system has reached equilibrium. For each solid-liquid coupling C_{S-L}, we determine the force per unit length of the radial perimeter of the fiber in the z direction as a function of the distance from the bottom of the fiber. The increment in z is taken as the distance between adjacent layers of the fiber, so that each value calculated corresponds to the force acting on a single layer. We then average these values over the configurations generated at equilibrium to produce the complete distribution of forces along the fiber. Two examples, for couplings $C_{S-L} = 0.8$ and 1.0, are given in Fig. 4. Because we measure the forces in the z direction, attractive forces between the liquid and the solid have a minus sign.

Figure 4 confirms that, as predicted, the forces are located entirely at the bottom of the fiber and in the area where the liquid-vapor interface meets the fiber, across the three-phase contact zone (TPZ). At the bottom of the fiber, we see that the first solid layer is repelled by the liquid (positive force); i.e., the liquid is trying to expel the fiber. However, the force on the second layer is attractive. The following layers do not provide any additional contribution until the TPZ is reached. The force then becomes progressively more attractive, reaching a maximum before smoothly vanishing once again.

Figure 5 shows the integrated force (a) at the bottom of the fiber and (b) across the TPZ for each solid-liquid coupling investigated, plotted as a function of the associated equilibrium contact angle. Also shown are solid lines representing γ_{LV} and $-\gamma_{LV}(1 + \cos\theta^0)$ based on the independent measurements of the contact angle and interfacial tension. Evidently, the forces at the two critical locations are in close agreement with theory over the very wide range of contact angles investigated. It is particularly notable that the force at the bottom of the fiber is almost exactly equal to the surface tension of the liquid and independent of the contact angle. The agreement with Eq. (5) is significantly better than that obtained previously with molecular dynamics [13]. Moreover, since Eq. (5) is derived via Young's equation, the latter's validity appears

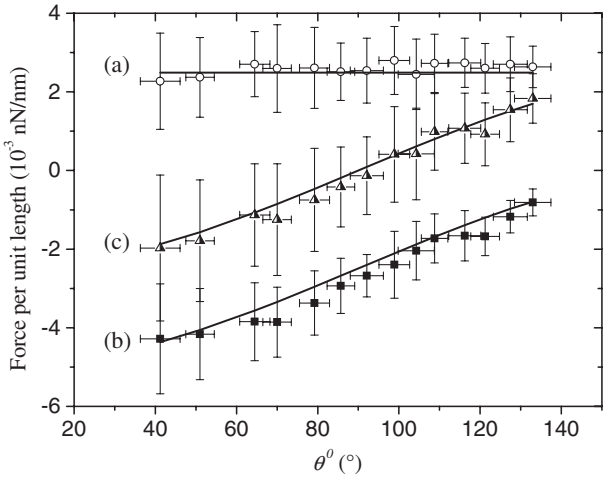

FIG. 5. The total force (a) at the bottom of the fiber and (b) across the three-phase zone for $C_{S-L} = 0.4$ to 1.05, plotted as a function of the equilibrium contact angle. The solid lines through the data represent (a) γ_{LV} and (b) $-\gamma_{LV}(1 + \cos\theta^0)$. (c) The intermediate plot compares the sum of the measured forces at both locations with that predicted by Eq. (3): $-\gamma_{LV}\cos\theta^0$ (because we measure the forces in the z direction, attractive forces between the liquid and the solid have a minus sign).

to be confirmed at the scale of the simulations. Further support is provided by (c) the intermediate plot in Fig. 5. This directly compares the sum of the forces measured at the two locations (i.e., the net force) with that predicted by Eq. (3): $-\gamma_{LV}\cos\theta^0$ (because we measure the forces in the z direction, attractive forces between the liquid and the solid have a minus sign). The latter is indicated by the solid line through the data. The excellent agreement justifies the use of Young's equation in the AFM experiments with nanofibers and nanocones. In each case, the lines through the data lie well within error bars based on the standard deviation of the data.

Strictly speaking, our simulations have not really proved Young's equation, since we have measured neither γ_{SL} nor γ_{SV}. What we have measured is their difference, or more particularly what Gibbs [2] called the superficial tension of the liquid in contact with the solid $\varsigma_{LS} = \gamma_{SL} - \gamma_S$, where γ_S is the surface tension of the bare solid in contact with a vacuum and the solid is assumed to be immutable, i.e., unaffected by the fluid phase with which it is in contact. The liquid in our simulations is essentially nonvolatile, due to the use of eight-atom chains, so the part of the fiber that is not immersed is in contact with a vacuum. It may, therefore, be assumed to have the thermodynamic surface tension γ_S. Furthermore, the solid is sufficiently rigid as to be effectively immutable, as required by Gibbs. Thus, what we have really demonstrated is that $\varsigma_{LS} = \gamma_{LS}\cos\theta^0$.

Conclusions.—This Letter describes the use of large-scale molecular dynamics simulations to measure the tangential force distribution along nanoscale fibers dipped into a liquid meniscus together with independent measurements of the equilibrium contact angle θ^0 and the liquid-vapor interfacial tension γ_{SV}. The results confirm that the force at the contact line is equal to $\gamma_{LV}(1 + \cos\theta^0)$ and that there is an additional force at the base of the fiber equal to γ_{LV}. This yields a net force $\gamma_{SV} - \gamma_{SL}$. Moreover, the force $\gamma_{LV}\cos\theta^0$ exerted by the liquid-vapor interface at the contact line is equal to this same net tangential force. Taken together, these results provide compelling evidence that the use of Young's equation is justified at the nanoscale and, in particular, in wetting experiments with carbon nanotubes and nanocones [8,9].

This research has been partially funded by the Interuniversity Attraction Poles Programme (IAP 7/38 MicroMAST) initiated by the Belgian Science Policy Office, the Région Wallonne, and the FNRS.

*david.seveno@umons.ac.be

[1] T. Young, Phil. Trans. R. Soc. London **95**, 65 (1805).
[2] J. W. Gibbs, *The Collected Works of J. Willard Gibbs* (Yale University, London, 1957).
[3] R. E. Johnson, Jr., J. Phys. Chem. **63**, 1655 (1959).
[4] P. Roura and J. Fort, J. Colloid Interface Sci. **272**, 420 (2004).
[5] T. Ingebrigtsen and S. Toxvaerd, J. Phys. Chem. C **111**, 8518 (2007).
[6] J. H. Snoeijer and B. Andreotti, Phys. Fluids **20**, 057101 (2008).
[7] S. K. Das and K. Binder, Europhys. Lett. **92**, 26 006 (2010).
[8] A. H. Barber, S. R. Cohen, and H. D. Wagner, Phys. Rev. Lett. **92**, 186103 (2004).
[9] M. Delmas, M. Monthioux, and T. Ondarçuhu, Phys. Rev. Lett. **106**, 136102 (2011).
[10] A. Marchand, J. H. Weijs, J. H. Snoeijer, and B. Andreotti, Am. J. Phys. **79**, 999 (2011).
[11] A. Dupré, *Théorie Mécanique de la Chaleur* (Gauthier-Villars, Paris, 1869), p. 201.
[12] S. K. Das, A. Marchand, B. Andreotti, and J. H. Snoeijer, Phys. Fluids **23**, 072006 (2011).
[13] J. H. Weijs, B. Andreotti, and J. H. Snoeijer, Soft Matter **9**, 8494 (2013).
[14] A. Marchand, S. K. Das, J. H. Snoeijer, and B. Andreotti, Phys. Rev. Lett. **109**, 236101 (2012).
[15] M. J. de Ruijter, T. D. Blake, and J. De Coninck, Langmuir **15**, 7836 (1999).
[16] G. Martic, J. De Coninck, and T. D. Blake, J. Colloid Interface Sci. **263**, 213 (2003).
[17] D. Seveno, G. Ogonowski, and J. De Coninck, Langmuir **20**, 8385 (2004).
[18] E. Bertrand, T. D. Blake, and J. De Coninck, J. Phys. Condens. Matter **21**, 464124 (2009).
[19] D. F. James, J. Fluid Mech. **23**, 325 (1965).
[20] J. G. Kirkwood and F. P. Buff, J. Chem. Phys. **17**, 338 (1949).
[21] E. Salomons and M. Mareschal, J. Phys. Condens. Matter **3**, 3645 (1991).